

Active Control of a Round Jet Using Two Unsteady Microjets

P. Zhang¹, Y. Zhou¹ and Md. Mahbub Alam²

¹Department of Mechanical Engineering
 The Hong Kong Polytechnic University, Hong Kong

²ShenZhen Graduate School, Harbin Institute of Technology,
 University Town, Shenzhen, China

Abstract

Unsteady microjets are used to control the mixing performance of a round jet at a Reynolds number of 8000. Two microjets were placed at diametrically opposite locations upstream of the nozzle exit. We explored the effects of the mass rate ratio C_m and forcing frequency ratio f_{ex}/f_0 of the microjets on the primary jet, where f_{ex} is the microjet forcing frequency and f_0 the predominant vortex frequency in the free jet. The C_m and f_{ex}/f_0 examined are 0 ~ 15.4% and 0 ~ 1.28, respectively. The flow was measured using hot wire, flow visualization and particle imaging velocity techniques in two orthogonal planes through the jet axis. The jet centreline decay rate exhibits a strong dependence on f_{ex}/f_0 . Given $f_{ex}/f_0 \approx 1.0$, this decay rate displays three types of distinct behaviours for C_m investigated in terms of the response of large-scale coherent structures to the control, which is different from previous studies. The flow physics and control mechanisms are explored.

Introduction

As one of the typical basic shear flows, the jets are widely seen in engineering, e.g. in aero and automobile engines, burners used in various industries and power plants, water-jet machining, electronic equipment cooling, printing and drying. Naturally, their manipulation or control for mixing enhancement has received a great deal of attention in the literature. The concept to use control jets to enhance jet mixing was proposed by Davis [3]. Seidel et al. [15] emulated the performances of noncircular jets by placing around a round main jet multiple steady radial blowing jets at positions where the corners or vortices would be if noncircular nozzles were used. Their results agreed surprisingly well with those of corresponding noncircular jets [11], indicating that a jet may be controlled, based on fluidic means, to achieve the optimized performance under different operation conditions. Please refer to Henderson [5] for a recent review on the implementation of microjets for jet control.

This work is a continuation of the study by Zhou et al. [17], who deployed two steady microjets to manipulate a round jet. The Reynolds number was made the same for the two investigations. So is the jet control facility, though two diametrically opposite unsteady microjets were used presently. Along with an exploration on control mechanisms, the dependence of jet decay on f_{ex} and C_m of unsteady microjets is investigated, where f_{ex} is the microjet forcing frequency and C_m is the mass rate ratio of the microjets to the main jet.

Experimental Details

Air Jet Facility

The jet facility consists of two parts, namely, main-jet and microjet assemblies (figure 1). The main jet is produced by a compressed air supply of a constant pressure of 5 bar gauge

pressure, as are the microjets. As shown in figure 1a, once entering a large mixing box, air is mixed with seeding particles, when PIV measurement is conducted; it passes through a tube, a plenum box, a 300-mm-long diffuser of 15° half-angle and two fine screens (7 mesh/cm) before reaching a cylindrical settling chamber of 400 mm in length and 114 mm in diameter. The nozzle contraction follows a contour specified by equation $R = 57 - 47\sin^{1.5}(90 - 9x/8)$, as used by Mi et al. [12]; the contraction ratio is 32.5 with an exit diameter of $D = 20$ mm. The nozzle was extended by a 47-mm-long smooth circular passage of the same diameter D . The jet issues into an air-conditioned spacious laboratory. The exit Reynolds number $Re_D = U_e D/\nu$ of the main jet is fixed at 8000, where $U_e = 6$ m/s is the centreline velocity in the exit plane and ν is kinematic viscosity. The predominant vortex frequency f_0 is 143.5 Hz measured near the potential core end of the free jet.

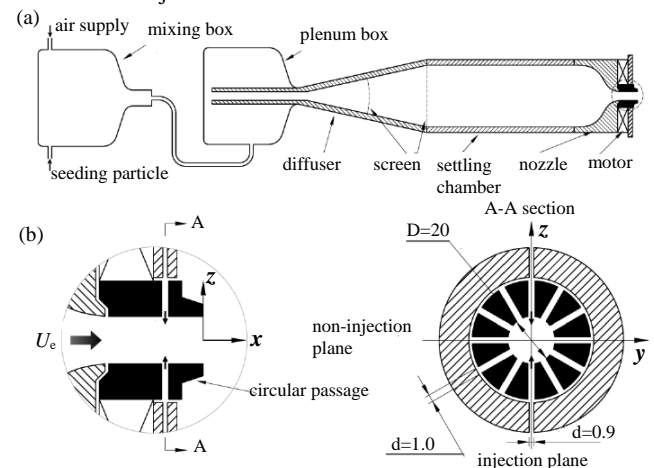


Figure 1. Schematic of the air jet facility with an unsteady microjet excitation system: (a) the main jet assembly, (b) microjet assembly.

The control jet is provided by unsteady microjets. The microjet assembly (figure 1b) comprises a stationary and a rotating disk. The stationary disk is drilled with 6 orifices of 0.9 mm in diameter and distributed azimuthally at 60-deg interval. These orifices are connected through short and equal-length tubes to a chamber. The rotating disk is drilled with 12 orifices of 1 mm in diameter, azimuthally equally spaced, which are 17 mm upstream of the exit. The rotating disk is the rotor of a servo motor with a maximum speed of $N = 2950$ r.p.m.. Once the orifices on the stationary and the rotating disks are aligned during rotation, a pulsed microjet is emitted towards the main jet axis as shown in figure 1(b). Two in-phase unsteady microjets were presently used to manipulate the primary jet. The frequency f_r of the rotating disk is equal to $N/60$ and the microjet pulsation frequency f_{ex} is then $12N/60$, corresponding to a frequency range of 0 to 590 Hz, covering the vortex frequency in the free jet. The flow rates of

both main jet and control microjets are adjustable independently via two separate flowmeters, whose experimental uncertainty is no more than 1%.

The origin of the coordinate system is chosen at the centre of the circular passage exit (figure 1b). The x axis is along the streamwise direction, the (x, y) plane is the non-injection plane orthogonal to the injection plane, i.e. the (x, z) plane that the two radial microjets lie in.

Flow Diagnostic Techniques

A single hotwire was used to measure the streamwise fluctuating velocity u . The sensing element was made of a 1-mm-long tungsten wire of 5 μm in diameter. The wire was operated on a constant temperature circuit at an overheat ratio of 1.8. The signal from the wire was offset, low-pass filtered at a cut-off frequency of 2.8 kHz, and then sampled at a frequency of 6 kHz using a 12-Bit A/D converter. The sampling duration for each record was 80 s, which was sufficient to ensure the *rms* value of u to be within a 1% uncertainty. The hotwire probe was mounted on a computer-controlled two-dimensional traversing mechanism with a resolution of 0.01mm longitudinally and laterally. The hot wire was calibrated in the potential core of the free jet using a Pitot-static tube connected to an electronic micromanometer (Furness FCO510).

A DANTEC planar PIV system (Flowmap) was deployed to visualize the flow in the injection and non-injection planes. The flow was seeded with smoke generated using a TSI oil droplet generator. The averaged seeding particle size was around 1 μm . Flow illumination was provided by the dual light sheets of about 1 mm thickness produced by two New wave standard pulsed laser sources of a 532 nm wavelength, each with a maximum energy output of 120 mJ/pulse. Particle images were captured using one CCD camera (double frames, 2048 \times 2048 pixels). The nozzle exit plane was painted black to minimize noise due to light reflection. The PIV image covers an area of 217 mm \times 217 mm. Under light reflection from the nozzle, the active image area was reduced to 1998 \times 2048 pixels. Velocity vectors generated based on spatial adaptive correlation amount to 62,238 (246 \times 253), and the interrogation area is 32 \times 32 pixels with a 75% overlap along both directions. A total of 1400 pairs of images were captured in each plane. It has been confirmed that the mean velocity and turbulent intensity both have uncertainty of no more than 1%.

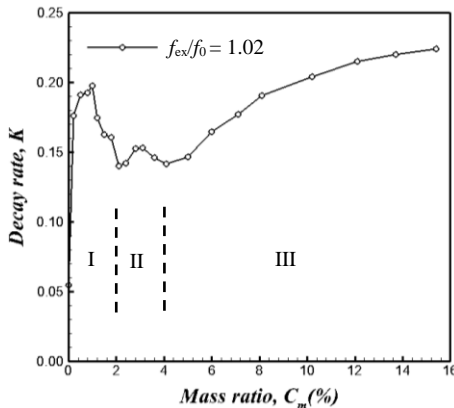


Figure 2. Dependence of the jet decay rate K on the mass ratio C_m of the microjets to the main jet under the forcing frequency ratio of $f_{ex} / f_0 = 1.02$.

Presentation of Results

Dependence of Jet Decay Rate on the Mass Ratio

Following Zhou et al. [17], the jet decay rate K is estimated by $(U_e - U_{5D}) / U_e$, where U_e is the centreline velocity in the jet exit and U_{5D} is the centreline velocity at $x/D = 5$. Figure 2 presents the

dependence of K on C_m which varies from 0 to 15.4% at a given frequency ratio of $f_{ex} / f_0 = 1.02$. Note that, with increasing C_m , K climbs rapidly to a local maximum of 0.2 and then drops to 0.14 at $C_m = 2\%$. The gradual asymptotic rise in K as C_m exceeds 4.0% is similar to the observation by Parekh et al. [14] who deployed two pulsed slot jets of C_m less than 2% to enhance the centreline velocity decay of a round jet for $Ma = 0.23$, where Ma is the Mach number at the jet exit.

The present jet response (figure 2) may be divided into three types, i.e., I ($C_m < 2.0\%$), II ($C_m = 2.0\sim 4.0\%$), and III ($C_m > 4.0\%$). The flow displays distinct flow characteristics in these types, as illustrated below at $C_m = 0.8\%$ and 1.6% in type I, 3.4% in type II, and 10.4% & 15.4% in type III. Figure 3 presents the momentum thickness θ of jet in the three types, defined by

$$\theta(x) = \int_{R_{0.99}}^{R_{0.01}} \frac{U}{U_c(x)} \left(1 - \frac{U}{U_c(x)}\right) dr \quad (1)$$

where $U_c(x)$ is the local centreline velocity, $R_{0.01}$ is the radius at $U/U_c = 0.01$ and $R_{0.99}$ the radius at $U/U_c = 0.99$. The θ in the free jet shows a relatively broad plateau at $x/D < 2.0$, which is linked to the stage prior to the shear layer rollup to form vortices, and then increases quite rapidly first and then less so. On the other hand, θ under control grows appreciably faster. In the injection plane (figure 3a), when the mass ratio is small, i.e., $C_m = 0.8\%$ and 1.6% or in type I, a narrow plateau occurs in θ at $x/D \approx 2.0$,

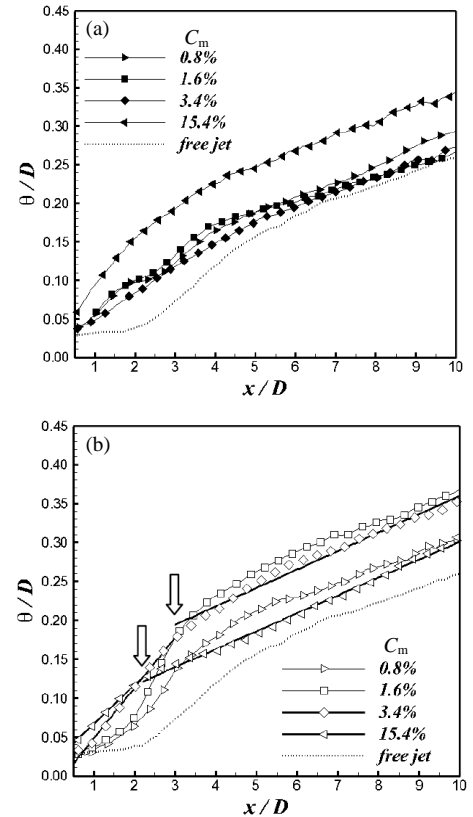


Figure 3. Dependence of momentum thickness in jet on x/D ($f_{ex} / f_0 = 1.02$): (a) injection plane; (b) non-injection plane.

which separates the θ growth into two distinct stages, as observed in controlled plane mixing layers and circular jets by Ho and Huang [6] and Laufer and Zhang [10]. The increase in θ upstream of the plateau results from the shear layer rollup under the periodic perturbation influence of microjets. The vortices are then formed and advected downstream without strong interference with each other initially for a very short distance, which is probably responsible for the narrow plateau. Further downstream, the vortices interact more vividly and their breakdown under the azimuthal instability as suggested by Browand and Laufer [1] and

probably other instabilities brings about a regrowth in θ . In contrast, θ in type II ($C_m = 3.4\%$) grows more linearly over the entire x/D examined. In type III, θ is significantly larger than those in types I & II. In the non-injection plane (figure 3b), θ under small C_m in types I & II is characterized by a rather rapid increase over $x/D = 1.5 \sim 3.0$, which is referred to as a step-like rise by Ho and Huang [6] and Laufer and Zhang [10]. These authors ascribed this rise to vortex pairing. The variation in θ with x/D in type II consists of two nearly linear regions with the dividing point at $x/D \approx 3.0$, as marked by an arrow in figure 3b. Similar observation is made in type III, though with the dividing point shifted to $x/D \approx 2.2$.

Dependence of Jet Decay Rate on the Forcing Frequency

As shown in figure 4, the decay rate at $C_m = 0.8\%$ is strongly dependent on f_{ex}/f_0 , showing a twin-peak variation, one ($K = 0.144$) at $f_{ex}/f_0 = 0.66$ and the other ($K = 0.215$) at $f_{ex}/f_0 = 0.89$, along with a trough ($K = 0.130$) at $f_{ex}/f_0 = 0.77$ between the twin peaks. A similar observation was made by Cheng et al. [2] who used piezoelectric ceramic actuators to control vortex shedding from a square cylinder. The periodic excitation may enhance, if in-phase, or weaken, if out-of-phase, vortices, resulting in the pronounced peak and the trough, respectively.

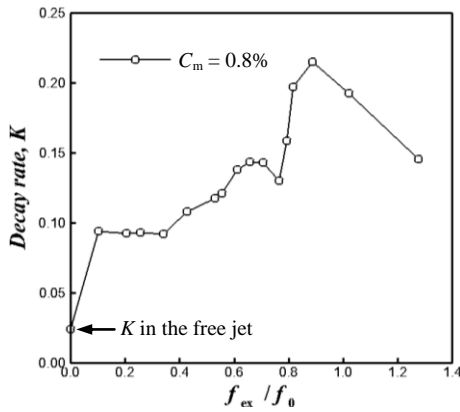


Figure 4. Dependence of the decay rate on the microjet forcing frequency at $C_m = 0.8\%$.

Discussion

It is now well established that jet entrainment and decay are closely associated with the large-scale coherent structures in shear flows (e.g. Dimotakis et al. [4] and Ho and Huerre [7] and Hussain [8,9]). Thus, we examine the variation in the flow structure captured in flow visualization with C_m and f_{ex}/f_0 .

Figure 5 shows the typical flow structure images captured in the controlled jet ($f_{ex}/f_0 = 1.02$) for the three types, along with that of the free jet. Except for the case of $C_m = 10.2\%$ (figure 5f & g), the rollup and presence of coherent structures are evident for $x/D < 3.0$. Vortex pairing is also discernible in the non-injection plane, as marked in figure 5c & e. Due to microjet forcing, vortices near the exit appear to be appreciably larger in scale in the injection plane (figure 5b & d) than in the free jet (figure 5a). Furthermore, the potential core appears greatly shortened. On the other hand, vortices are relatively small in size in the non-injection plane (figure 5c & e). Zaman and Hussain [16] found experimentally that a pure-tone acoustic excitation at relatively low amplitude could bring about weak coherent structures. It is worth noting that, at larger C_m in type II ($C_m = 3.4\%$), vortices are not so evident $x/D > 1.0$ (figure 5d). The earlier transition to turbulence corresponds to a more linear growth in θ (figure 3a).

The vortex pairing observed in the non-injection plane (figure 5c & e) deserves attention. Two neighbouring vortex rings at $x/D = 1.5$ ($C_m = 0.8\%$, figure 5c) are undergoing a phase of mutual

induction during a typical vortex pairing after the shear layer rolls up into vortices owing to Kelvin-Helmholtz instability. Similar vortex interactions also take place in the case of $C_m = 3.4\%$ (figure 5e). One may wonder why the vortex pairing occurs in the non-injection plane when C_m is small. Experiments on a forced mixing layer using a periodic excitation by Oster and Wygnanski [13] indicated that monochromatic excitation at very low amplitude tends to trigger the merging of neighbouring small eddies but the flow at higher amplitude consisted of a train of large structures without interacting with each other, which agrees well with our observations.

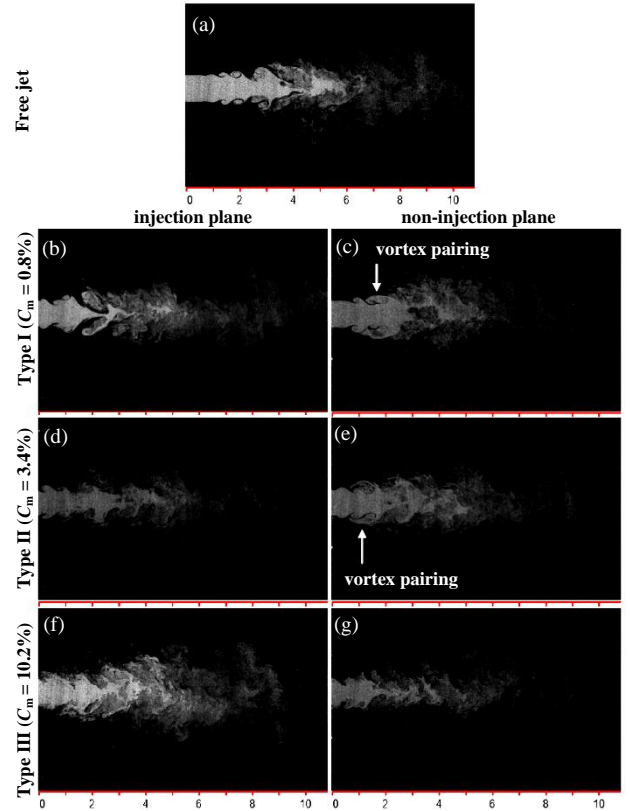


Figure 5. Photographs of typical flow structures captured from flow visualization in the free jet and the controlled jet ($f_{ex}/f_0 = 1.02$) for different types. The flow is from left to right.

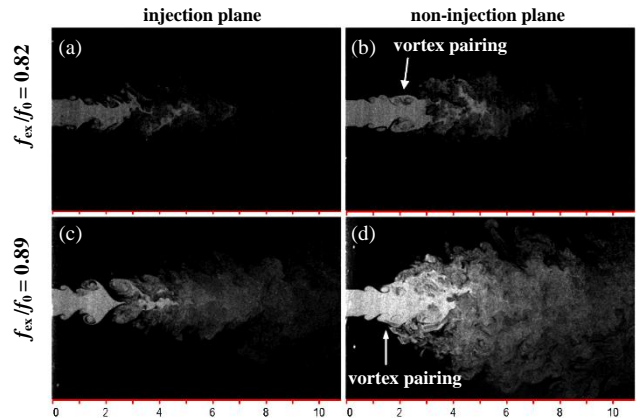


Figure 6. Photographs of typical flow structures captured from flow visualization in the controlled jet ($C_m = 0.8\%$) for different f_{ex}/f_0 .

At $C_m = 10.2\%$ (type III), the flow appears turbulent in both planes even at $x/D = 0$ (figure 5f & g). At large C_m , the two microjets in the injection plane penetrate deeply into the potential core, as observed by Davis [3], and even clash with each other around the centreline. The strong disturbance is partially

transferred into the non-injection plane, eventually leading to the transition of laminar vortices to the turbulent in both planes. Being turbulent, the vortices entrain more ambient fluid into the jet and thereby recover a high value of K in type III, as suggested by Zhou et al. [17]. Thus, with increasing C_m , the jet gradually approaches a fully turbulent state with a bell-shaped rather than a top-hat mean velocity profile at jet exit and K approaches an asymptotic value.

There is no doubt that f_{ex}/f_0 has a crucial influence upon the flow structure. Figure 6 shows the typical flow structure of the controlled jet ($C_m = 0.8\%$) under the excitation of $f_{ex}/f_0 = 0.82$ and 0.89 . In the injection plane vortices appear inhibited at $f_{ex}/f_0 = 0.82$ (figure 6a). In the non-injection plane, the vortex pairing is observed over $x/D = 1 \sim 2$ for all the cases of $f_{ex}/f_0 = 0.82, 0.89$, and 1.02 (figures 6b & d, figure 5c). Note that at the given C_m (0.8%), the jet spread is much wider in the non-injection plane at $f_{ex}/f_0 = 0.89$ (figure 6d) than those at $f_{ex}/f_0 = 0.82$ and 1.02 (figure 6b, figure 5c), internally consistent with the largest K at $f_{ex}/f_0 = 0.89$ (figure 4).

Conclusions

The following conclusions may be drawn out of the investigation:

1) The effects of the mass ratio on the control performance can be divided into three types. Type I corresponds to very small mass ratio, and the perturbation excites the natural instability of the jet, leading to significantly enhanced or weakened vortices, along with vortex pairing. The jet decay or entrainment rate is greatly modified and the control is highly effective. For Type III, the mass ratio is large and the two control jets penetrate deeply into the potential core and even clash with each other, resulting in the transition of laminar vortices to a turbulent state in both planes. The jet decay rate increases and approaches an asymptotic state with increasing C_m , though the control may be less efficient than Type I. Type II is a transition between I and III, characterized by a medium mass ratio.

2) The jet decay rate depends strongly on the forcing frequency, showing one pronounced peak and one trough. The excitation can greatly enhance vortices, contributing to the peak in the decay rate dependence and may impair vortices, resulting in the trough.

3) At relatively large mass ratio (Types II & III), the jet decay rate experiences two linear phases of different growth rates in the non-injection plane, with the dividing point at $x/D = 2 \sim 3$.

Acknowledgments

YZ wishes to acknowledge support given to him from Research Grants Council of HKSAR through grant PolyU 5350/10E.

References

- [1] Browand, F. K. & Laufer, J., The Role of Large Scale Structures in the Initial Development of Circular Jets, in *4th Symp. Turbulence in Liquids*, editors J. L. Zakin and G. K. Patterson, Science Press, 1975, 333-344.
- [2] Cheng, L., Zhou, Y. & Zhang, M. M., Perturbed Interaction between Vortex Shedding and Induced Vibration, *J. Fluid. Struct.*, **17**, 2003, 887-901.
- [3] Davis, M. R., Variable Control of Jet Decay, *AIAA J.*, **20(5)**, 1982, 606-609.
- [4] Dimotakis, P. E., Miake-Lye, R. C. & Papantoniou, D. A., Structure and Dynamics of Round Turbulent Jets, *Phys. Fluid.*, 1983, **26(11)**, 3185-3192.
- [5] Henderson, B., Fifty Years of Fluidic Injection for Jet Noise Reduction, *International J. Aeroacoustics*, **9**, 2010, 91-122.
- [6] Ho, C. M. & Huang, L. S., Subharmonics and Vortex Merging in Mixing Layers, *J. Fluid Mech.*, **119**, 1982, 443-473.
- [7] Ho, C. M. & Huerre, P., Perturbed Free Shear Layers, *Ann. Rev. Fluid Mech.*, **16**, 1984, 365-424.
- [8] Hussain, A. K. M. F., Coherent Structures and Turbulence, *J. Fluid Mech.*, **173**, 1986, 303-356.
- [9] Hussain, A. K. M. F., Coherent Structures - Reality and Myth, *Phys. Fluid*, **26(10)**, 1983, 2816-2850.
- [10] Laufer, J. & Zhang, J. X., Unsteady Aspects of a Low Mach Number Jet, *Phys. Fluid*, **26(7)**, 1983, 1740-1750.
- [11] Mi, J., Nathan, G. J. & Luxton, R. E., Centreline Mixing Characteristics of Jets from Nine Differently Shaped Nozzles, *Exp. Fluids*, **28**, 2000, 93-94.
- [12] Mi, J., Nobes, D. S. & Nathan, G. J., Influence of Jet Exit Conditions on the Passive Scalar Field of an Axisymmetric Free Jet, *J. Fluid Mech.*, **432**, 2001, 91-125.
- [13] Oster, D. & Wygnanski, I., The Forced Mixing Layer between Parallel Streams, *J. Fluid Mech.*, **123**, 1982, 91-130.
- [14] Parekh, D. E., Kibens, V., Glezer A., Wiltse, J. M. & Smith, D. M., Innovative Jet Flow Control: Mixing Enhancement Experiments, in *34th AIAA Aerosp. Sci. Meet.*, American Institute for Aeronautics and Astronautics, 1996, *Pap.* 96-0308.
- [15] Seidel, J. F., Pappart, C., New, T. H. & Tsai, H. M., Effects of Multiple Radial Blowing around a Circular Jet, in *43th AIAA Aerosp. Sci. Meet.*, American Institute for Aeronautics and Astronautics, 2005, *Pap.* 2005-0866.
- [16] Zaman, K. B. M. Q. & Hussain, A. K. M. F., Natural Large-Scale Structures in the Axisymmetric Mixing Layer, *J. Fluid Mech.*, **138**, 1984, 325-351.
- [17] Zhou, Y., Du, C., Mi, J. & Wang, X. W., Turbulent Round Jet Control Using Two Steady Minijets, *AIAA J.*, **50(3)**, 2012, 736-740.